Supporting Information for:

On-Surface Growth Dynamics of Graphene Nanoribbons: The Role of Halogen Functionalization

Marco Di Giovannantonio,[1] Okan Deniz,[1] José I. Urgel,[1] Roland Widmer,[1] Thomas Dienel,[1,#] Samuel Stolz,[1] Carlos Sánchez-Sánchez,[1,†] Matthias Muntwiler,[2] Tim Dumslaff,[3] Reinhard Berger,[4] Akimitsu Narita,[3] Xinliang Feng,[4] Klaus Müllen,[3] Pascal Ruffieux,[1] Roman Fasel[1,5,*]

[1]*Empa - Swiss Federal Laboratories for Materials Science and Technology - nanotech@surfaces Laboratory, 8600 Dübendorf, Switzerland*
[2]*Paul Scherrer Institute, 5232 Villigen, Switzerland*
[3]*Max Planck Institute for Polymer Research, 55128 Mainz, Germany*
[4]*Center for Advancing Electronics Dresden and Department of Chemistry and Food Chemistry, Technische Universität Dresden, 01062 Dresden, Germany*
[5]*Department of Chemistry and Biochemistry, University of Bern, 3012 Bern, Switzerland*

Content

1. Additional experimental data

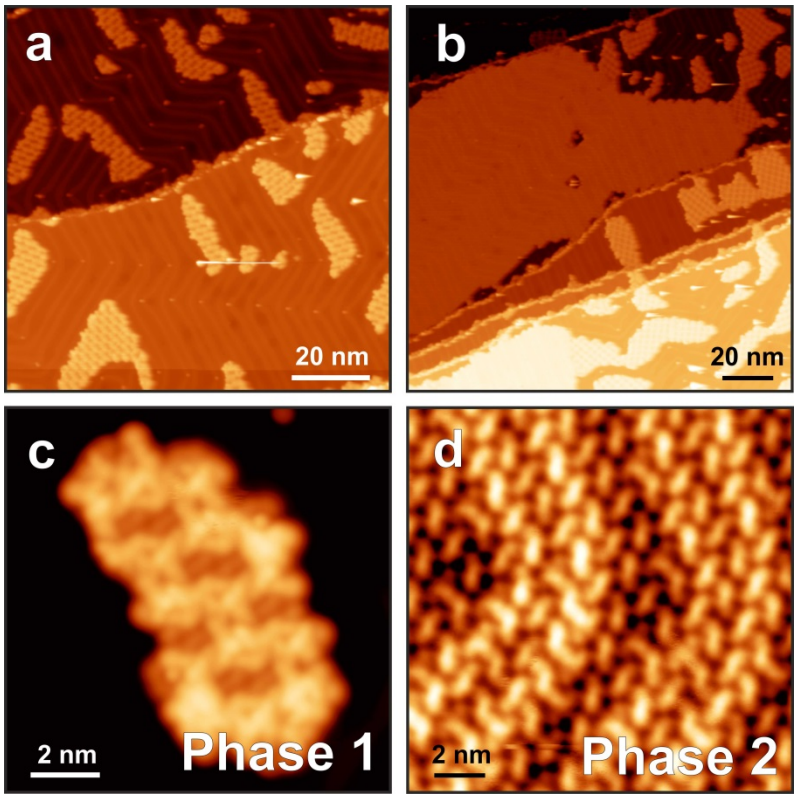

Figure S1. STM images after RT deposition of DITP at low coverage (0.1 ML, images a and c, V_b = –1.7 V, I_t = 5 pA) and medium coverage (0.4 ML, images b and d, V_b = –1.7 V, I_t = 10 pA). Only phase 1 is present at low coverage, while phase 2 appears at higher coverage, forming large islands (magnified images of the two phases are reported in c and d). At 0.4 ML coverage, phase 2 dominates over phase 1 (70% and 30%, respectively).

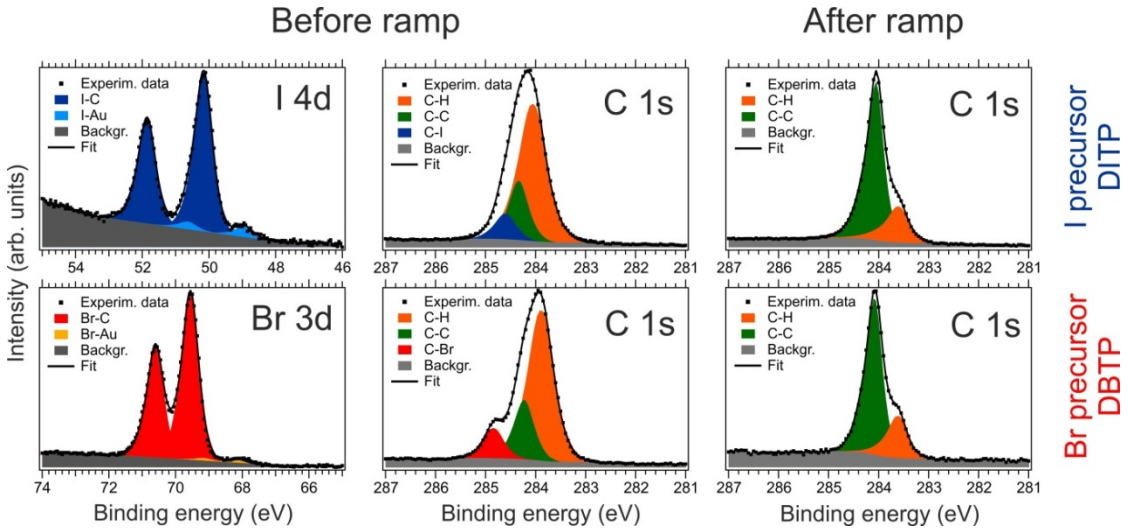

Figure S2. High-resolution XPS spectra of the halogen and carbon core levels acquired before and after each fast-XPS map with photon energy 425 eV. The molecules adsorb mostly intact on the Au(111) surface at RT, with only 7% (2%) of iodine (bromine) already detached from the precursor molecules. The relative intensity of the fitting components confirms that DITP and DBTP are present at RT, while 9-AGNRs are formed after the annealing at about 450 ºC. The fitting parameters are reported in Table S1.

Table S1. Fitting parameters of the fits reported in Figure S2.

		Component	Line shape	Binding Energy (eV)	Doublet separation (eV)	Full width at half maximum (eV)	Relative amount (%)
DITP	I $4d_{5/2}$ before ramp	I-C	Voigt	50.17	1.7	0.67	93
		I-Au	Voigt	48.99	1.7	0.67	7
	C 1s before ramp	C-H	Asymmetric Voigt	284.05		0.62	67
		C-C	Asymmetric Voigt	284.34		0.46	22
		C-I	Asymmetric Voigt	284.60		0.51	11
	C 1s after ramp	C-H	Asymmetric Voigt	283.61		0.47	22
		C-C	Asymmetric Voigt	284.05		0.36	78
DBTP	Br $3d_{5/2}$ before ramp	Br-C	Voigt	69.58	1.0	0.62	98
		Br-Au	Voigt	68.23	1.0	0.62	2
	C 1s before ramp	C-H	Asymmetric Voigt	283.89		0.58	67
		C-C	Asymmetric Voigt	284.23		0.47	22
		C-Br	Asymmetric Voigt	284.84		0.46	11
	C 1s after ramp	C-H	Asymmetric Voigt	283.61		0.43	24
		C-C	Asymmetric Voigt	284.08		0.36	76

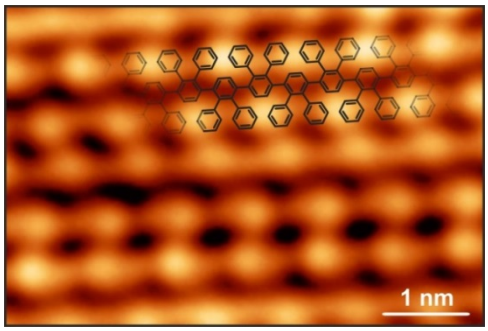

Figure S3. STM image of DITP after RT deposition and annealing at 160 ºC showing the polymer phase (V_b = –1.5 V, I_t = 10 pA). The model of a polymer chain is superimposed to the image. Each bright protrusion is due to two adjacent tilted phenyls, as described in our previous work.[1]

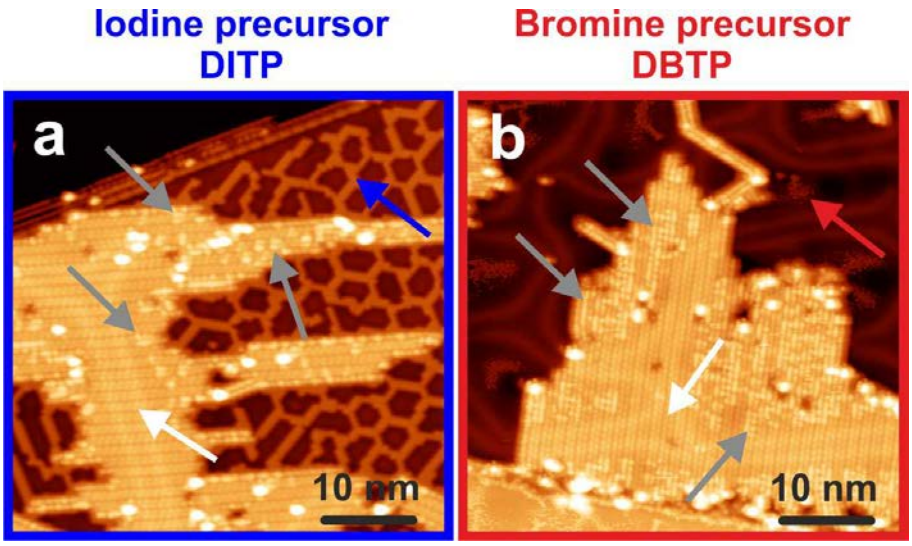

Figure S4. STM image of DITP (a) and DBTP (b) after RT deposition on Au(111) and annealing at 160 ºC and 220 ºC, respectively. Scanning parameters: V_b = –1.5 V, I_t = 10 pA (a); V_b = –1.3 V, I_t = 30 pA (b). The images are acquired at 5 K (a) and 77 K (b). In both cases, the halogens are detached from the precursor molecules and bind to the Au surface (blue and red arrows). Bromine atoms are imaged as fuzzy moieties because of their mobility at 77 K. Some protrusions are observed within polymer islands (grey arrows). We attribute these features to a partial amount of halogen atoms which is intercalated between the polymers and the gold surface. In these areas, the herringbone reconstruction of the surface is suppressed, indicating that the presence of halogens strongly bound to the gold. However, the herringbone reconstruction is visible in the regions without halogens (white arrows).

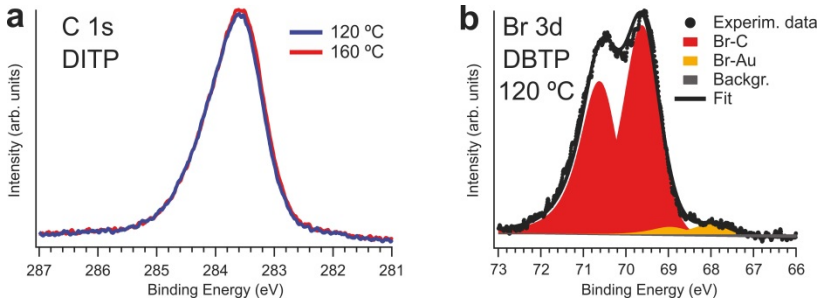

Figure S5. XPS spectra obtained from horizontal profiles of the fast-XPS maps. C 1s and Br 3d spectra are extracted from the maps in Figure 2f and Figure 2c, respectively. In the case of DITP, our STM images after annealing the surface at 160 ºC show that polymers are formed, and the photoelectron spectra of such polymers show a well-defined line shape (a). This line shape is identical to the one observed at 120 ºC, suggesting that no further chemical modifications occur in the molecular nanostructures above 120 ºC (until the cyclodehydrogenation starts at 280 ºC) and that we have polymers in the range 120 – 280 ºC. In contrast, DBTP is still unreacted at 120 ºC, as demonstrated by the absence of any chemical shift in the C 1s signal in Figure 2e and by the fit reported in panel b: here, only 6 % of the bromine atoms are detached from the precursors and bind the gold substrate, while the remaining 94 % of the molecules are still intact. This demonstrates that the polymerization temperatures of the two monomers are indeed different.

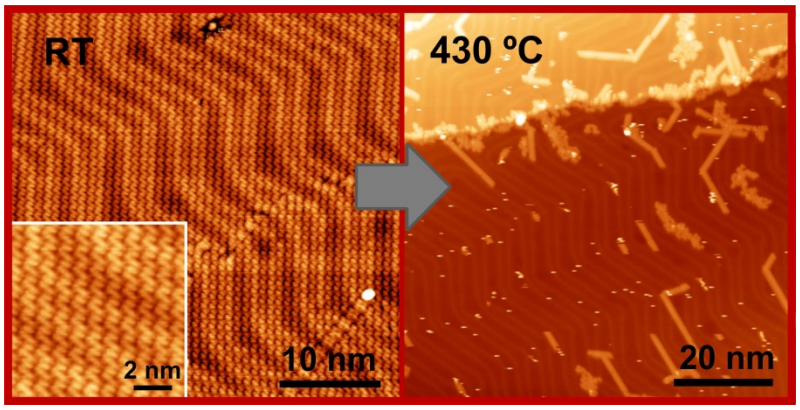

Figure S6. STM images of Au(111) after RT deposition of the DBTP precursor (left panel, V_b = –1.5 V, I_t = 70 pA) and after annealing the surface to 430 ºC with a constant heating rate of 0.2 ºC·s^{-1} (right panel, V_b = –1.5 V, I_t = 50 pA), showing that a strong desorption of the molecules takes place during the annealing, which results in a low coverage of 9-AGNRs on the surface at the end of the reaction.

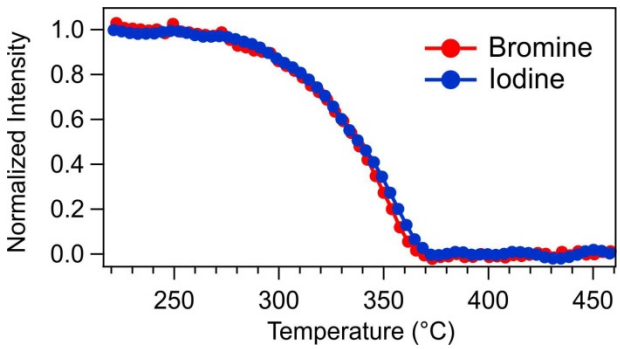

Figure S7. Total area of the Br 3d and I 4d signals acquired in the fast-XPS measurements. The sample containing DITP has been prepared as described in the main text, while the sample containing DBTP has been prepared by depositing the monomers on the Au(111) surface held at 200 ºC, with a 4-fold increased deposition time compared to the standard RT deposition. This allows to compensate the partial monomer desorption, and to produce a surface with a comparable amount of polymers and Au-bound bromine atoms than in the DITP case. Ac-

cording to these results, the desorption of Br and I atoms from the gold surface follow identical kinetics. This suggests that an additional mechanism is triggering halogen desorption, because simple atomic or associative desorption is expected to occur at different temperatures for different halogens. We suggest that gold atoms of the surface might play a role in this process.

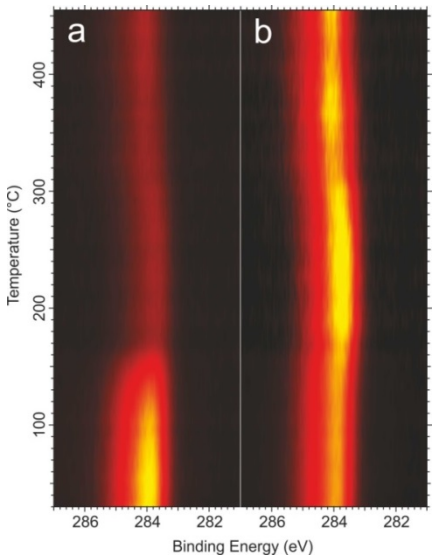

Figure S8. C 1s fast-XPS map acquired after deposition of DBTP on Au(111). The original map (raw data) and the map after line-by-line normalization by the total area are reported in a and b, respectively.

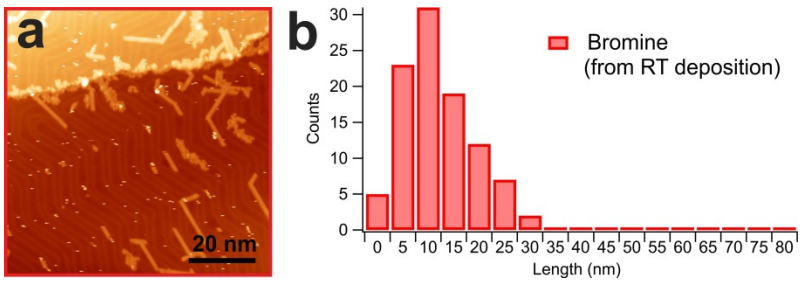

Figure S9. STM image (a) and length histogram (b) for 9-AGNRs obtained from DBTP deposited on Au(111) at RT. The histogram is obtained from about 100 ribbons. The observed average length is similar to that reported in Figure 3c in the main text, confirming that the different sample preparations discussed for the samples reported in Figure 3 are not affecting our interpretation, *i.e.* 9-AGNRs fabricated with the DITP precursor are systematically longer than the ones from DBTP. STM image parameters: $V_b = -1.5$ V, $I_t = 50$ pA.

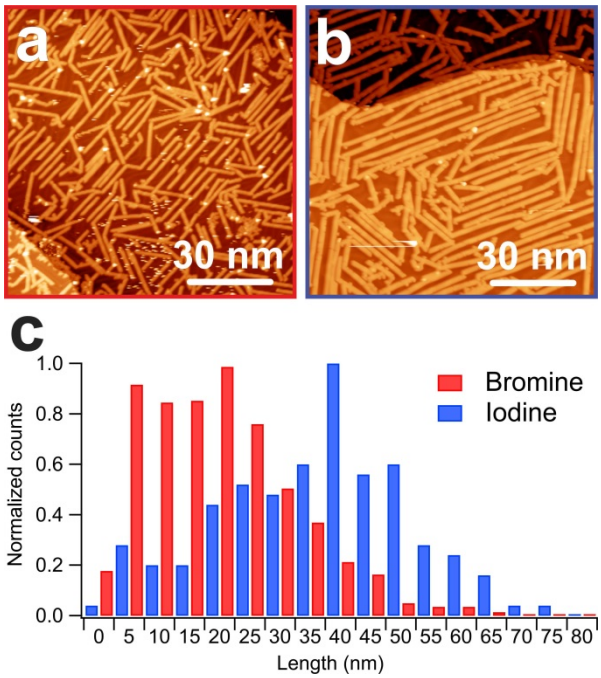

Figure S10. STM images showing different length of 9-AGNRs obtained from DBTP (a) and DITP (b) with similar surface coverage (a: V_b = –1.8 V, I_t = 30 pA, b: V_b = –1.5 V, I_t = 10 pA). The histograms in c report the length distribution measured for the two systems using large-scale STM images and measuring about 800 and 140 ribbons in the case of DBTP and DITP, respectively. The histograms have been normalized for easy comparison.

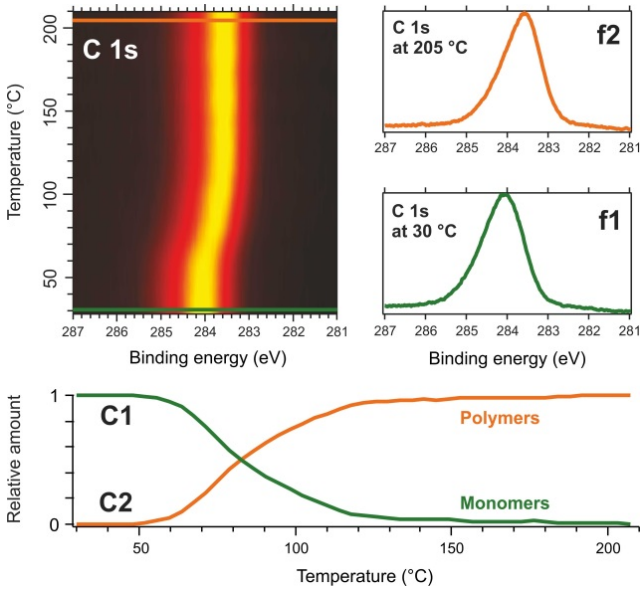

Figure S11. Schematic representation of the fitting procedure adopted to extract the kinetic curves from fast-XPS maps. As an example, the low-temperature region of the C 1s fast-XPS map for the DITP precursor is reported in the top left panel. Two horizontal profiles of the map before and after the transition produce the two fitting functions f1 and f2 (green and orange, respectively). Then, every horizontal line of the map is fitted with the function Y = C1·f1 + C2·f2 and the coefficients C1 and C2 are plotted as a function of temperature (bottom panel), representing the relative amount of each specie as a function of temperature.

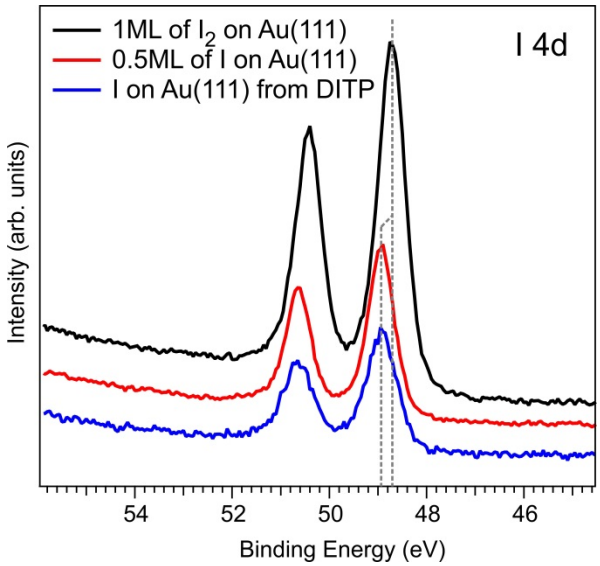

Figure S12. I 4d XPS spectra. The black curve is measured after deposition of 1 ML of molecular iodine (I_2) from the gas phase on Au(111) at RT. Heating the surface to about 240 ºC induces partial desorption of the iodine, the remaining showing a chemical shift of 250 meV toward higher binding energy (red curve). This shift is attributed to the dissociation of molecular iodine into gold-chemisorbed atomic iodine, which is confirmed by comparison with the XPS acquired after dehalogenation of DITP molecules on Au(111) (blue curve). The background lines of the three curves have been vertically shifted for a better comparison. These spectra confirm that the desorption of pure iodine from Au(111) can be directly compared to the desorption of iodine detached from DITP (see Figure 4 in the main text).

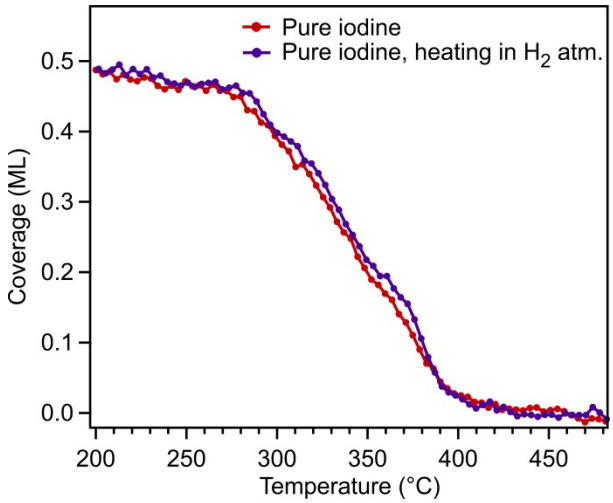

Figure S13. Kinetic curves extracted from I 4d fast-XPS maps of about 0.5 ML of atomic iodine on Au(111). The two curves refer to the standard heating procedure (red) and to the heating in the presence of $3 \cdot 10^{-8}$ mbar molecular hydrogen in the vacuum chamber (purple). The graph demonstrates that the residual hydrogen in the vacuum chamber has no effect on the iodine desorption kinetics.

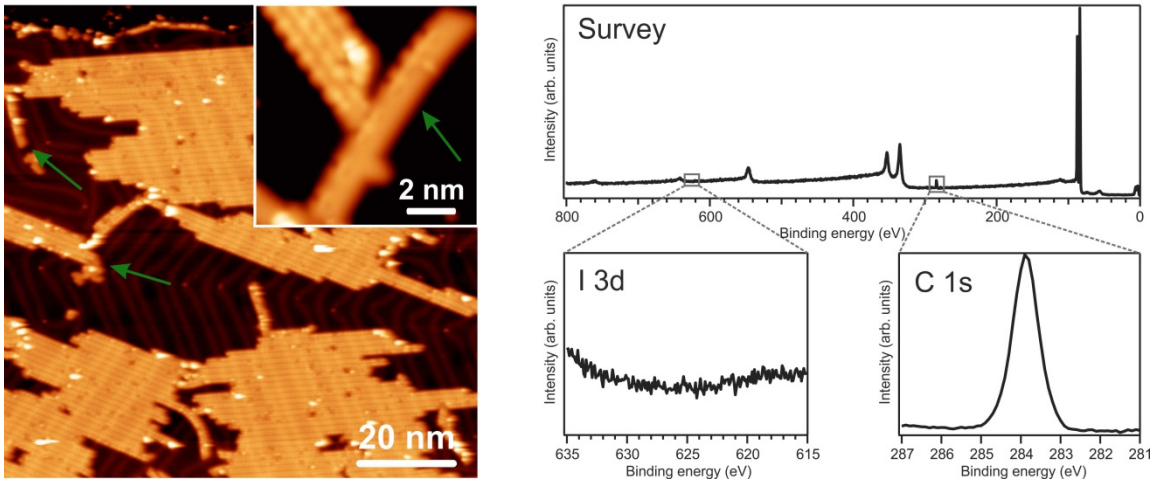

Figure S14. STM image of the Au(111) surface after deposition of DITP molecules at RT and annealing to 270 ºC for 20 minutes (left panel), and XPS spectra of the as-prepared sample (right panels). The STM image is acquired at 5K (V_b = –1.5 V, I_t = 10 pA). Iodine is desorbed from the surface and polymers are still not converted into GNRs (also confirmed by XPS measurements). The inset in the left panel shows a partially cyclodehydrogenated chain (V_b = 1.0 *V*, I_t = 30 pA). XPS analysis of this sample was performed in-house, using monochromatized Al Kα X-rays and a hemispherical electron analyzer equipped with a multi-channel plate detector. The spectra were acquired with 200 eV pass energy in transmission mode. Two possible mechanisms could justify the observed result: (i) the desorption of iodine as AuI is enabled by the longer annealing time at the temperature corresponding to the onset of its desorption (compare Figure 3 in the main text), or (ii) the small amount of cyclodehydrogenated chains (indicated by the green arrows) provide enough hydrogen to activate the desorption of HI. The ratio of hydrogen atoms released by cyclodehydrogenation to iodine atoms is 4:1, therefore, 25 % of the polymers should be converted into GNRs to provide enough hydrogen to desorb all the iodine as HI. This STM image clearly shows that this is not the case, supporting thus mechanism (i).

2. Fit of the kinetic curves

In this section we discuss the fitting of the kinetic curves shown in Figure 4 in the main text according to a derivation of the Polanyi-Wigner equation:

$$\frac{d\theta}{dT} = -A\frac{\theta^n}{r}e^{\left(-\frac{E}{k_B T}\right)} \qquad (1)$$

where dθ/dT is the desorption rate (ML·s^{-1}), θ is the coverage (ML), T is the temperature (K), A is the attempt frequency (s^{-1}), n is the reaction order, r is the heating rate (K·s^{-1}), E is the energy barrier of the process (eV) and k_B is the Boltzmann constant.

Equation (1) represents the reaction rate for a desorption process as a function of temperature upon surface heating with constant heating rate (see curves in the top panels of Figure S12). The integral of this function provides the coverage vs temperature relation (see curves in the bottom panels of Figure S12), which is used to fit our kinetic curves (Figure S13).

To fit the kinetic curves, two different equations have been used:

$$\frac{d\theta}{dT} = -A\frac{\theta^n}{r}e^{\left(-\frac{E}{RT}\right)} - B \qquad (2)$$

$$\frac{d\theta}{dT} = -\left(A_1 \frac{\theta^{n_1}}{r} e^{\left(-\frac{E_1}{RT}\right)} + A_2 \frac{\theta^{n_2}}{r} e^{\left(-\frac{E_2}{RT}\right)}\right) - B \qquad (3)$$

where B is an additional term introduced to account for the linear slope that is sometimes observed at the beginning of some kinetic curves (B=0 corresponds to the absence of such slope). The fitting of the dehalogenation and polymerization curves (**1** and **2** in Figure S13) is performed using a single Boltzmann term (equation (2)), while the sum of two Boltzmann terms (equation (3)) is needed to fit the iodine desorption and cyclodehydrogenation curves (**3**, **4** and **5** in Figure S13).

Second order kinetics are found for the dehalogenation and polymerization processes (curves **1** and **2** in Figure S13), with an energy barrier of about 1.0 eV (reasonable for a process starting at about 320 K). A combination (sum) of two kinetics is needed to fit curves **3**, **4** and **5**. In the case of iodine desorption enhanced by the presence of hydrogen (curve **3** in Figure S13), a second and a zero order process are found, with energy barriers of about 1.8 eV and 2.0 eV, respectively. The fits of curves **4** (desorption of pure iodine) and **5** (cyclodehydrogenation) require higher reaction order (about 5-6) for at least one of the two processes, with about 1.8 eV energy barrier, together with a first-order process with about 2 eV energy barrier.

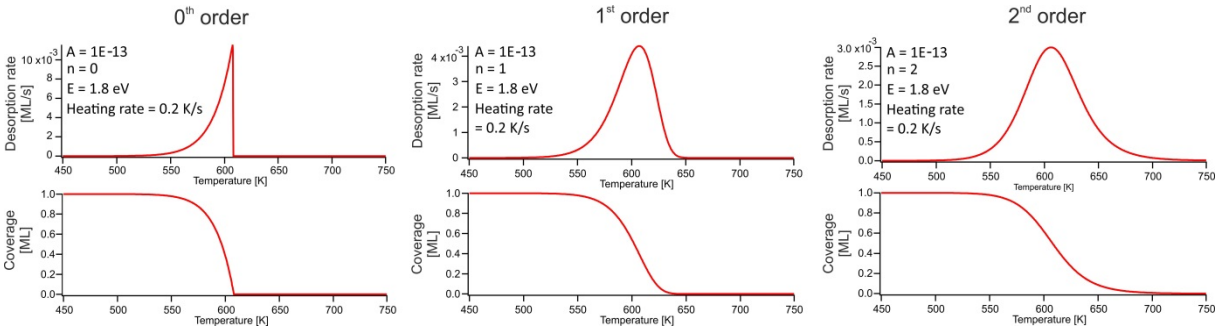

Figure S15. Model curves representing the desorption rate (TPD-like curves) and the coverage as a function of sample temperature for three different desorption orders. Equation (1) is used to plot the desorption rate (derived from the Polanyi-Wigner equation). The curves for the coverage vs temperature (bottom line of figure) have been obtained by integrating equation (1). The parameters used to plot each curve are given as insets. The same model has been used to fit the kinetic curves in Figure S13.

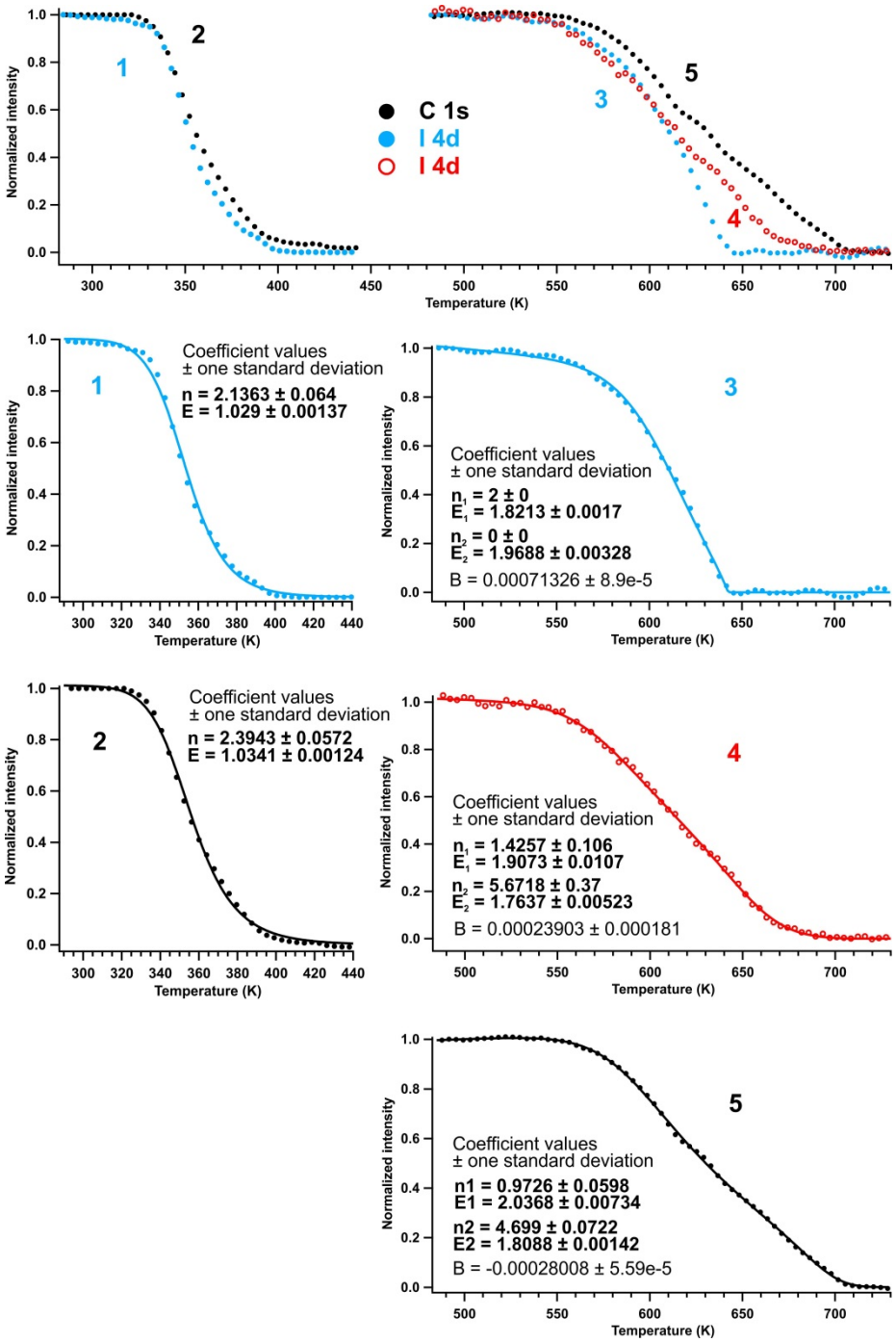

Figure S16. Fit of the kinetic curves (coverage vs temperature) reported in Figure 4 in the main text. The maximum intensity of each signal is due to the corresponding surface coverage before the reaction and has been normalized to 1. The integral of equation (2) is used as fitting function for curves **1** and **2**, while the integral of equation (3) is used as fitting function for curves **3**, **4** and **5**. The corresponding fitting coefficients are reported as insets. The term accounting for the initial slope (B) is reported only when different from zero. In all cases the initial coverage θ is 1 ML, the attempt frequency A is 10^{13} s^{-1} and the heating rate r is 0.2 $K \cdot s^{-1}$, and these values are kept fixed in the fitting. We tried to use different values of the attempt frequency (A), without any significant change in fit quality. In the fitting of curve **3**, the values of n_1 and n_2 have been kept fixed.

3. Monomer synthesis and characterizations

a. Materials and methods

Materials were purchased from Activate Scientific, Aldrich, Acros, ABCR, Merck, and Chempur, and used as received without further purification. Reactions dealing with air- or moisture-sensitive compounds have been carried out in a dry reaction vessel under argon atmosphere. Preparative column chromatography was performed on silica gel from Merck with a grain size of 0.063-0.200 mm (silica gel). NMR spectra were measured on Bruker DRX500 spectrometers, and referenced to residual signals of the deuterated solvent (Abbreviations: s = singlet, d = doublet, dd = double doublet, t = triplet, m = multiplet). High-resolution time-of-flight mass spectrometry (TOF MS) was performed on a SYNAPT G2 Si instrument (Waters Corp., Manchester, UK) with matrix-assisted laser desorption/ionization (MALDI) or atmospheric pressure photoionization (APPI) source. For MALDI-TOF MS, samples were mixed with tetracyanoquinodimethane (TCNQ) and dropped on a MALDI sample plate. The mass spectrometer was calibrated against red phosphorus under MALDI mode beforehand and the spectra were recorded using C_{60} as lock mass. Melting points were measured with a Büchi melting point detector. The temperature was increased in 5 °C·min^{-1} steps.

b. Synthetic routes

The synthesis of 3′,6′-dibromo-1,1′:2′,1″-terphenyl (DBTP) is described elsewhere.[1]
The synthesis of 3′,6′-diiodo-1,1′:2′,1″-terphenyl (DITP) is reported below.

Scheme S1: Synthetic route towards 3′,6′-diiodo-1,1′:2′,1″terphenyl (DITP)[a]

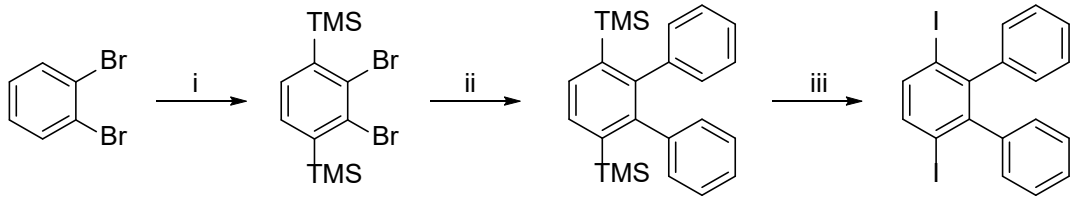

[a]Reagents and conditions: (i) *n*-BuLi, HN-(*i*-Pr)$_2$, TMS-Cl, THF, –78 °C, 5 h, 55%; (ii) $Pd_2(dba)_3$, SPhos, K_3PO_4, Toluene, 100 °C, 8 h, 97%; (iii) ICl, dichloromethane (DCM), 0 °C, 1 h, 98%

c. Synthesis steps

(2,3-Dibromo-1,4-phenylene)bis(trimethylsilane) (2)

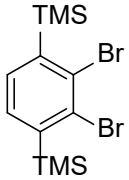

To a 500 mL round bottom flask, 15 mL of dry tetrahydrofuran (THF) was added and cooled to –78 °C under argon. At this temperature, *n*-butyllithium (*n*-BuLi) (1.6 M in *n*-hexane, 63.9 mL, 0.10 mol) and *N,N*-diisopropylamine (HN-(*i*-Pr)$_2$) (14.3 mL, 0.10 mol) were added subsequently. After 15 min of stirring, the resulting solution was slowly added to a solution of 1,2-dibromobenzene (10.0 g, 0.0424 mol) and TMS-chloride (11.1 g, 0.10 mol) in 20 mL of THF at –78 °C. The reaction mixture was stirred at this temperature for 5 h and quenched with diluted sul-

furic acid. The resulting mixture was diluted with water and extracted with diethyl ether. The combined organic layers were dried over magnesium sulfate and evaporated. The residue was dissolved in a mixture of acetone and methanol (1:1, 10 mL) and crystallized at–30 °C for several days to afford the title compound as a colorless solid in 55% yield. All spectral data was in accordance with the literature.[2]
^{1}H NMR (500 MHz, tetrachloroethane-d_2) δ 7.35 (s, 2H), 0.41 (s, 18H).
^{13}C NMR (126 MHz, tetrachloroethane-d_2) δ 145.56, 133.92, 133.14, –0.45.

3',6'-Bis(trimethylsilyl)-1,1':2',1''-terphenyl (3)

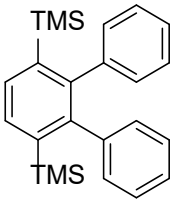

(2,3-Dibromo-1,4-phenylene)bis(trimethylsilane) (1.21 g, 3.18 mmol), potassium phosphate (4.05 g, 19.1 mmol), tris(dibenzylideneacetone)dipalladium(0) ($Pd_2(dba)_3$) (0.15 g, 0.16 mmol) and 2-dicyclohexylphosphino-2′,6′-dimethoxybiphenyl (SPhos) (0.13 g, 0.32 mmol) were dissolved in 25 mL of dry toluene and bubbled with argon for 45 min. The resulting mixture was stirred under argon for 8 h at 100 °C and then diluted with water and extracted with ethyl acetate. After removal of the organic solvents, the residue was purified by silica gel column chromatography with pure hexane as the eluent to obtain the title compound in 97% yield as a colorless powder.
M.P.: 116 – 118 °C
^{1}H NMR (500 MHz, tetrachloroethane-d_2) δ 7.62 (s, 1H), 7.10 – 7.03 (m, 6H), 7.00 – 6.93 (m, 4H), –0.06 (s, 18H).
^{13}C NMR (126 MHz, tetrachloroethane-d_2) δ 147.01, 142.12, 139.54, 132.38, 130.85, 126.53, 125.85, 0.42.
HRMS (MALDI-TOF, positive) *m*/*z* calculated for $C_{24}H_{30}Si_2$ $[M]^+$ 374.1886, found 374.1879

3',6'-diiodo-1,1':2',1''-terphenyl (4)

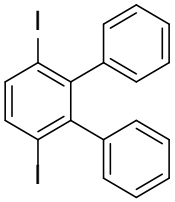

3',6'-Bis(trimethylsilyl)-1,1':2',1''-terphenyl (1.02 g, 2.67 mmol) was dissolved in 40 mL of dry dichloromethane (DCM) under argon and cooled to 0 °C. A solution of iodine monochloride (ICl) in DCM (0.50 M, 13.9 mL, 6.9 mmol) was added dropwise under light exclusion. After 1 h at 0 °C, the reaction mixture was quenched with sodium sulfite and the solvent was distilled completely. The residue was recrystallized from ethanol several times to obtain the title compound in 98% yield as colorless needles.
M.P.: 207 – 209 °C
^{1}H NMR (500 MHz, tetrachloroethane-d_2) δ 7.66 (s, 2H), 7.18 – 7.10 (m, 6H), 6.94 – 6.93 (m, 4H).
^{13}C NMR (126 MHz, tetrachloroethane-d_2) δ 146.57, 143.72, 139.23, 129.39, 127.37, 126.92, 100.88.
HRMS (MALDI-TOF, positive) *m*/*z* calculated for $C_{18}H_{12}I_2$ $[M]^+$ 481.9028, found 481.9035.

d. NMR spectra

^{1}H NMR (500 MHz, top) and ^{13}C NMR (126 MHz, bottom) spectra of **2** at 298 K in tetrachloroethane-d_2.

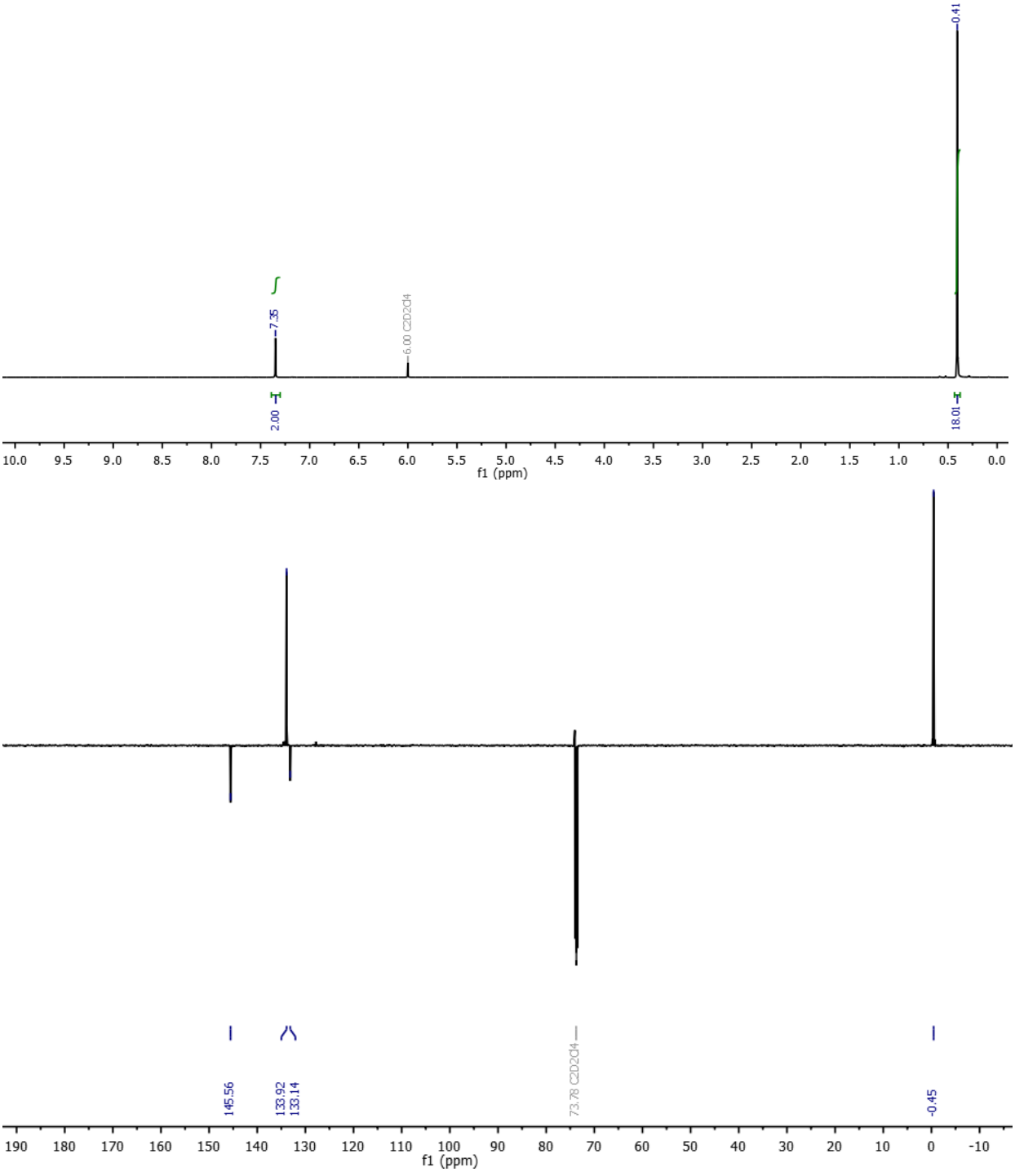

^{1}H NMR (500 MHz, top) and ^{13}C NMR (126 MHz, bottom) spectra of **3** at 298 K in tetrachloroethane-d_2.

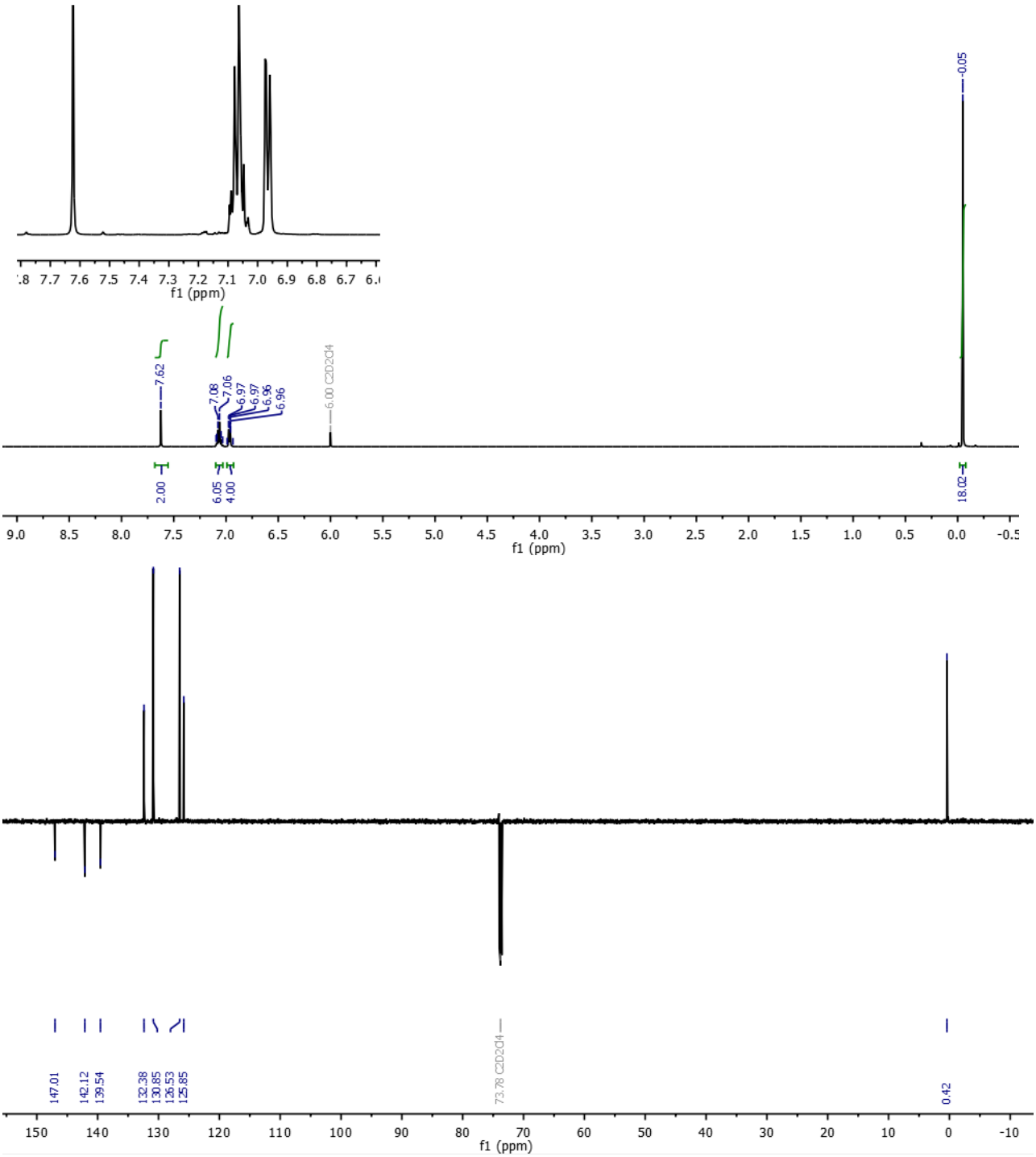

^{1}H NMR (500 MHz, top) spectrum of **4** at 298 K in tetrachloroethane-d_2.

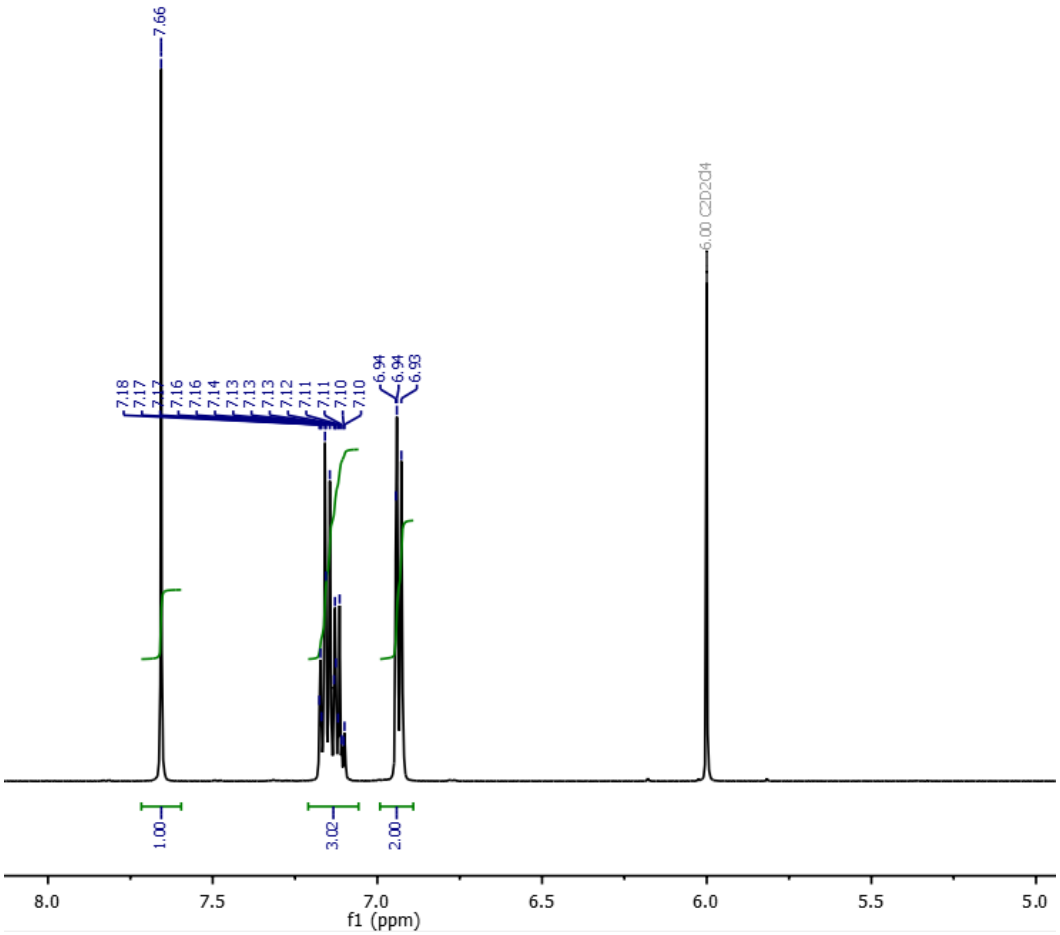

References

(1) Talirz, L.; Söde, H.; Dumslaff, T.; Wang, S.; Sanchez-Valencia, J. R.; Liu, J.; Shinde, P.; Pignedoli, C. A.; Liang, L.; Meunier, V.; Plumb, N. C.; Shi, M.; Feng, X.; Narita, A.; Müllen, K.; Fasel, R.; Ruffieux, P. On-Surface Synthesis and Characterization of 9-Atom Wide Armchair Graphene Nanoribbons. *ACS Nano* **2017**, *11*, 1380–1388.